BIOCHEMISTRY
including biophysical chemistry & molecular biology
Article

Biochemistry **2010,** *49,* 3083–3091 3083
DOI: 10.1021/bi902072f

A Flexible Bipartite Coiled Coil Structure Is Required for the Interaction of Hexim1 with the P-TEFb Subunit Cyclin T1[†]

André Schönichen,[‡,⊥] Janna M. Bigalke,[‡] Claus Urbanke,[§] Stephan Grzesiek,[∥] Sonja A. Dames,[∥] and Matthias Geyer*[,‡]

[‡]*Max-Planck-Institut für molekulare Physiologie, Abteilung Physikalische Biochemie, Otto-Hahn-Strasse 11, 44227 Dortmund, Germany,* [§]*Medizinische Hochschule Hannover, Biophysikalische Chemie, Carl Neuberg Strasse 1, 30625 Hannover, Germany, and* [∥]*Biozentrum Basel, Department of Structural Biology, University of Basel, Klingelbergstrasse 70, 4056 Basel, Switzerland.* [⊥]*Present address: Department of Cell and Tissue Biology, University of California, 513 Parnassus Ave., San Francisco, CA 94143.*

Received December 3, 2009; Revised Manuscript Received March 8, 2010

ABSTRACT: Transcription elongation is regulated by the cellular protein Hexim1, which inhibits phosphorylation of RNA polymerase II by interacting with the positive transcription elongation factor P-TEFb. Hexim1 binds directly to Cyclin T1 of P-TEFb with its coiled coil domain that is subdivided into a highly polar N-terminal segment containing nonconservative residues in the dimer interface and a C-terminal segment with an evolutionarily conserved sequence composition. Here we show that the noncanonical sequence composition of the first coiled coil segment is required for the interaction with Cyclin T1 while the second segment keeps the Cyclin T-binding domain dimeric upon binding. Both coiled coil segments exhibit distinct melting points as shown by heat denaturation experiments using circular dichroism spectroscopy. Deletion of the central stammer motif (Δ316−318) leads to a single denaturation reaction, suggesting formation of a continuous coiled coil. Mutation of noncanonical coiled coil residues K284 and Y291 to valines in the dimer interface of the first segment only slightly increases its stability. Concomitantly, deletion of the stammer but not the double point mutation led to a reduced affinity for Cyclin T1 as shown by isothermal titration calorimetry. Moreover, Cyclin T1 bound Hexim1 with a 1:2 stoichiometry, whereas truncation of the C-terminal coiled coil led to formation of an equimolar complex. These observations suggest that binding to Cyclin T1 induces an asymmetry or sterical hindrance in the first coiled coil segment of dimeric Hexim1 that disallows formation of a 2:2 complex as further supported by analytical ultracentrifugation and cross-linking experiments.

Transcription elongation is a critical step in gene expression and tightly regulated in eukaryotic cells (*1*). After transcription initiation, the production of nascent mRNA transcripts by RNA polymerase (pol) II requires phosphorylation of its carboxy-terminal domain (CTD).[1] Phosphorylation of serines in the multiple heptad repeats of the RNA pol II CTD releases the negative regulators and allows assembly of elongation factors with the mRNA processing machinery and chromatin remodeling factors (*2*). The specific hyperphosphorylation at position serine 2 of the CTD is mediated by cyclin-dependent kinase 9 (Cdk9) that together with a T-type cyclin (either Cyclin T1, T2, or K) forms the positive transcription elongation factor P-TEFb (*3*, *4*). In addition, P-TEFb phosphorylates the elongation repressor DRB sensitivity inducing factor (DSIF) and the negative elongation factor (NELF) for the activation of RNA pol II (*5*, *6*). While the active form of P-TEFb consists of two subunits, Cdk9 and CycT1, P-TEFb itself is tightly regulated and kept in an inactive state by the cellular protein Hexim (either Hexim1 or Hexim2) and a complex composed of the small nuclear 7SK RNA and its stabilizing factor Larp7 (*7*−*11*). Hexim directly binds by its central basic region to the 5′ hairpin loop of the 7SK RNA (*12*−*15*). Activation of P-TEFb in turn is achieved by bromodomain-containing protein 4 (Brd4) by a yet unknown mechanism (*16*−*19*).

The C-terminal Cyclin T-binding domain (TBD) of Hexim1 was shown to bind to the cyclin box domain of Cyclin T1 and to be required for inhibition of Cdk9 kinase activity in P-TEFb (*20*, *21*). Structural analysis revealed that the 12.5 kDa Hexim1-TBD protein forms a parallel dimeric coiled coil domain with an adjacent N-terminal short helix, connecting two chains of the 42 kDa Hexim1 protein to one functional unit (*22*). This coiled coil region is subdivided into a highly polar N-terminal segment that contains nonconservative residues in the dimer interface and a C-terminal segment that matches well the canonical sequence composition of a parallel coiled coil dimer. Left-handed coiled coil structures are characterized by a repeating pattern of seven residues, denoted $(\mathbf{abcdefg})_n$. Residues at positions **a** and **d** are typically nonpolar and form the oligomerization interface of the

[†]This work was supported by grants from the Deutsche Forschungsgemeinschaft to M.G. (GE-976/5) and from the Schweizer Nationalfonds to S.G. (SNF Grant 31-109712). S.A.D. was supported by a fellowship from the Treubel Fonds (Basel, Switzerland).

*To whom correspondence should be addressed. Phone: +49 (231) 133-2366. Fax: +49 (231) 133-2399. E-mail: matthias.geyer@mpi-dortmund.mpg.de.

[1]Abbreviations: Cdk, cyclin-dependent kinase; CTD, carboxy-terminal domain; CycT1, Cyclin T1; Hexim1, hexamethylene bisacetamide inducible protein 1; HIV-1, human immunodeficiency virus type 1; P-TEFb, positive transcription elongation factor b; SDS, dodecyl hydrogen sulfate; TBD, Cyclin T-binding domain; CD, circular dichroism; ITC, isothermal titration calorimetry; NMR, nuclear magnetic resonance; UV, ultraviolet.

Published on Web 03/08/2010

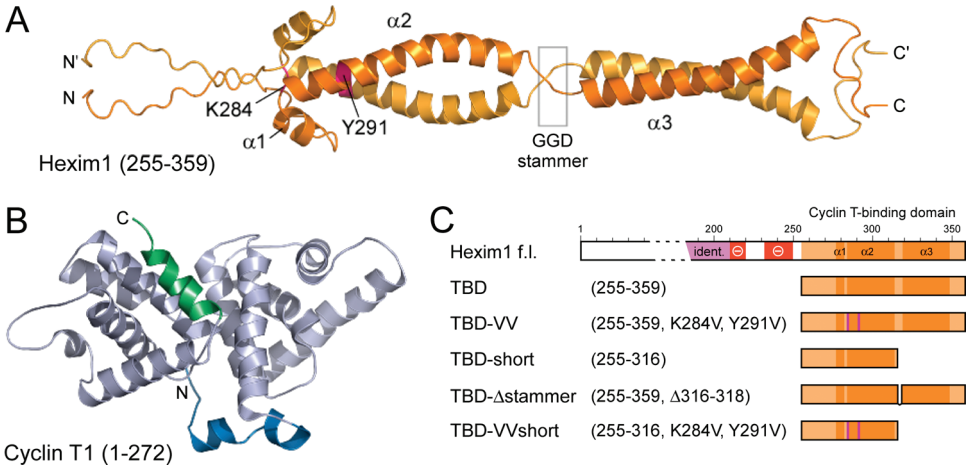

FIGURE 1: Structures of Cyclin T1 and Hexim1 interaction domains and schematic representation of protein constructs used in this study. (A) Solution structure of the dimeric Cyclin T-binding domain (residues 255−359) of human Hexim1 [Protein Data Bank entry 2GD7 (*22*)]. Residues K284 and Y291 positioned in the coiled coil interface are highlighted. The GGD stammer motif between both coiled coil segments is indicated. (B) Crystal structure of the cyclin box repeat domain (residues 1−272) of human Cyclin T1 [Protein Data Bank entry 2PK2 (*29*)]. N- and C-terminal helices that contribute considerably to the specificity of cyclins are colored blue and green, respectively. Both structures are drawn to scale. (C) Display of Hexim1 protein constructs used in this study. Besides the full-length protein, N- and C-terminal truncation mutants TBD and TBD-short were generated. TBD-Δstammer represents a deletion mutant of three residues (Δ316−318) that results in the formation of a continuous coiled coil structure. TBD-VV indicates the K284V/Y291V double point mutation at two successive **a** positions of the heptad repeats. Secondary structure elements are marked α1−α3.

helices, whereas residues at positions **e** and **g** are largely solvent-exposed, polar residues that guide the oligomerization specificity in the assembly of the periodic heptads through electrostatic interactions (*23*, *24*). Coiled coil structures typically range from monomeric to pentameric assemblies with a parallel or antiparallel orientation of the intertwined helices.

The canonical heptad repeats in the N- and C-terminal coiled coil segments of the Hexim1-TBD protein are interrupted by a sequence of 10 amino acids leading to a disruption of the helices (Figure 1A). While the first four residues (SKRL, positions 312−315) of this linker match the **abcd** consensus sequence for dimeric coiled coil sequences, the following central residues (GGD, positions 316−318) form an insert of three residues that interrupt the course of the intertwined helices. This so-called "stammer" typically leads to an overwinding of the supercoil (*25*), which was indeed observed in the Hexim1-TBD structure (*22*). The following three residues (DAR, positions 319−321) of this insert again correspond to the **efg** consensus requirements. The small size of the two inserted glycines in the stammer region contributes further to an increased flexibility between the two coiled coil segments. In addition, two highly conserved lysine and tyrosine residues at the core-forming **a** positions of the first two heptad repeats (K284 and Y291) vary from the ideal consensus sequence of a stable, dimeric coiled coil (*23*, *26*).

Recent structural analyses revealed the molecular basis of P-TEFb and Hexim1 proteins (*27*, *22*), but the mechanism of kinase inhibition by the cellular regulator remains elusive. Here we show that the flexibility of the first coiled coil segment in Hexim1 is required for its interaction with CycT1, while the C-terminal coiled coil segment keeps the Hexim1 protein dimeric. Deletion of the central stammer sequence that subdivides the coiled coil domain into two segments largely increases the stability of the helical domain but leads to a significant reduction in CycT1 binding affinity, although residues of the stammer do not contribute to direct interactions. We suggest that CycT1 interacts with the N-terminal coiled coil segment of Hexim1 by addition of a heterologous helix that together forms a tripartite assembly of two Hexim1 chains with one CycT1 subunit.

EXPERIMENTAL PROCEDURES

Plasmid Cloning, Protein Expression, and Purification. Plasmids encoding human Hexim1 (GenBank accession number AB021179) with domain boundary 1−359 (fl), 255−359 (TBD), or 255−316 (TBD-short) were generated by PCR-mediated amplification with a primer containing NcoI and EcoRI restriction sites. Site-directed mutagenesis of the K284V/Y291V double mutation (TBD-VV) and deletion of residues 316−318 that form the stammer between the two coiled coil segments (TBD-Δstammer) was performed using the megaprimer method with both sense and antisense oligonucleotides similarly as described previously (*28*). Fragments were cloned into prokaryotic expression vectors pProEx-HTa (Invitrogen) and pGEX-4T1 (GE Healthcare) modified with a TEV protease cleavage site. Cloning of the DNA encoding CycT1 (residues 1−272, 1−281, or 1−292) for expression as a GST fusion protein has been described previously (*21*, *29*).

Hexim1- and CycT1-encoding plasmids were transformed into *Escherichia coli* BL21(DE3) cells (Novagen). Proteins were typically expressed at 30 °C and purified as described previously (*21*, *28*). Fractions containing Hexim1-TBD proteins were concentrated to 1.0 mM in 20 mM KP_i buffer (pH 7.4), 50 mM NaCl, and 1 mM DTE and stored at −80 °C. Protein concentrations were determined by the Bradford assay (Bio-Rad) and extinction coefficient measurements. Protein concentrations always refer to the molecular weight of a monomer.

Isothermal Titration Calorimetry. Thermodynamic parameters of the CycT1−Hexim1 interaction were determined by isothermal titration calorimetry using a VP-ITC apparatus (MicroCal). Proteins were dialyzed against ITC buffer [50 mM Hepes (pH 7.5) and 100 mM KCl] prior to subjection. Typically, CycT1(1−272) at a concentration of 40 μM was thermostated in the sample cell at 15 °C, and Hexim1 proteins at 10-fold higher concentrations were injected from the syringe stepwise into solution by volumes of 8 μL. The change in heating power was observed for 4 min until equilibrium was reached before the next injection was started. Data were evaluated using the manufacturer's analysis software.

Analytical Gel Filtration. Analytical gel filtration experiments were performed with a multicomponent Waters 626 LC system using a Biosep-SEC-S2000 column (300 mm × 1.8 mm, Phenomenex) at a flow rate of 1.0 mL/min. Prior to injection of the protein samples, the column was equilibrated in 50 mM Hepes (pH 7.5), 100 mM KCl, and 1 mM TCEP buffer. Elution profiles were monitored by UV absorption at 280 nm. The void volume (V_0) was determined with blue dextran (Sigma). The column was calibrated with a protein standard (Bio-Rad) in a manner like that described previously (*30*). CycT1 and Hexim-TBD protein samples were dialyzed from frozen stocks into the equilibration buffer, diluted to a concentration of 1 mg/mL each, and injected onto the column at a volume of 90 μL. Protein complexes were incubated for 30 min prior to application on the column. Gel filtration experiments were performed repeatedly at room temperature.

Circular Dichroism Spectroscopy. CD spectra of Hexim1-TBD samples in the far-UV region (190−250 nm) were recorded on a Jasco J-815 spectropolarimeter using a quartz cuvette with a path length of 2 mm. Samples were dialyzed against 5 mM KP_i buffer (pH 8.0) and measured at concentrations of 5.0 μM. Spectra were recorded with a step size of 1 nm and an integration time of 1 s in a manner similar to that described previously (*31*). The raw CD signal (in millidegrees), after subtraction of the blank signal of the cuvette and buffer, was converted to mean residue ellipticity (in degrees squared centimeters per decimole). Temperature scanning CD measurements were taken with simultaneous monitoring of the temperature and molar ellipticity at 222 nm at a heating and cooling rate of 5.0 K/min. The temperature reading was at the heating/cooling disk that harbors the measurement cuvette. De- and renaturation spectra were averaged from three independent measurements. The first derivatives of the denaturation curves were obtained using ORIGIN version 7.0 and smoothed with a bipolynomial filter function before being fitted to a single or double Lorentzian line.

Chemical Cross-Linking Experiments. A mixture of 0.1 mM CycT1 (1−272) with either 0.1 mM Hexim1-TBD protein or TBD-short in 20 mM Hepes buffer (pH 8.0) and 100 mM NaCl was incubated in the presence of a 20-fold excess of cross-linking reagent BS^3 [bis(sulfosuccinimidyl)suberate, Thermo Scientific] for 30 min at room temperature. The reaction was quenched with 50 mM Tris to prevent unspecific aggregations. SDS sample buffer was added to this reaction mixture, and samples were analyzed by 18% SDS−PAGE.

Analytical Centrifugation and Sedimentation Velocity Experiments. Analytical ultracentrifugation experiments were performed with a Beckman/Coulter XLA analytical ultracentrifuge equipped with UV scanner optics using an eight-hole An-Ti analytical rotor. Sedimentation velocity experiments were conducted in double-sector centerpieces made of charcoal-filled Epon at a speed of 43000 rpm and 20 °C. Samples were scanned at 280 nm. The sedimentation boundary was analyzed using SEDFIT (*32*). This program uses a set of numerical solutions of Lamm's differential equation to transform the measured sedimentation profiles into a differential sedimentation coefficient distribution corrected for diffusional broadening by Fredholm integral transformation and regularizes this distribution using a maximum entropy procedure. The frictional ratio that relates the sedimentation coefficient to the diffusion coefficient is varied to fit the measured data. The sedimentation coefficient distributions were corrected for buffer viscosity and density using partial specific volumes of 7.356×10^{-4} m^3/kg for CycT1 and 7.193×10^{-4} m^3/kg for Hexim1 calculated from the respective amino acid composition using the increments given by SEDNTRP (*33*).

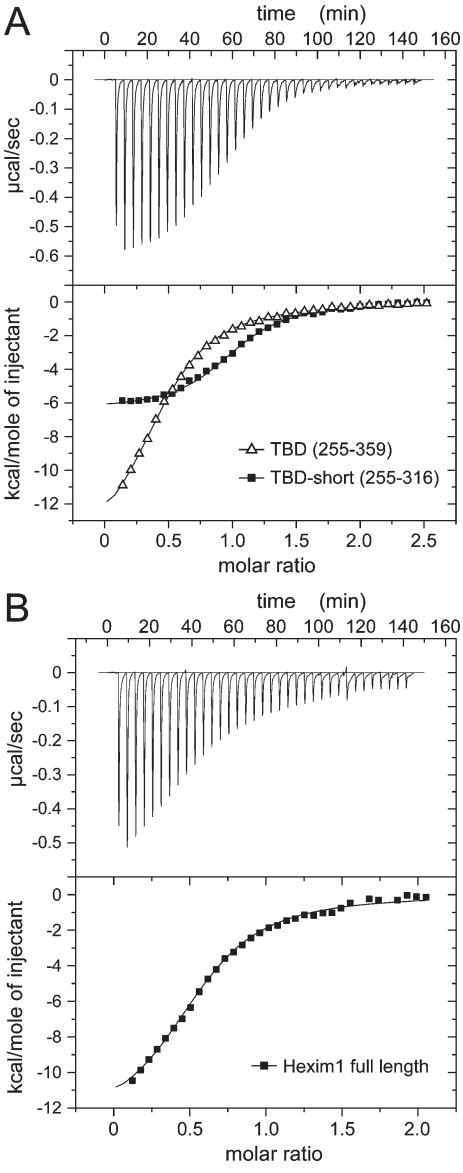

FIGURE 2: Binding affinity and stoichiometry of the Hexim1−CycT1 interaction analyzed by isothermal titration calorimetry. (A) ITC of CycT1 with Hexim1-TBD(255−359) or TBD-short(255−316). Both TBD molecules bound with similar affinities to CycT1. The interaction between CycT1 and TBD-short has a 1:1 molar ratio, while the molar ratio between CycT1 and TBD is 0.5, indicating that one CycT1 molecule binds a TBD dimer. The top panel displays the heat current of the CycT1 to TBD-short measurement. (B) ITC of CycT1 with full-length Hexim1 confirmed the 1:2 molar ratio of formation of the complex and revealed similar binding affinities as for TBD. The thermodynamic parameters of the interactions are listed in Table 1.

RESULTS

Molecular Basis of the Cyclin T1−Hexim1 Interaction. To analyze the molecular basis of the assembly of the complex of CycT1 and its regulator protein, Hexim1, we designed a set of different expression constructs (Figure 1). The structure of the C-terminal Cyclin T-binding domain (TBD) of Hexim1 consists of two coiled coil segments (α2/α2′ and α3/α3′) similar in length and a short α-helix (α1/α1′) that folds back onto the first coiled coil (Figure 1A). Besides full-length Hexim1(1−359), the constructs analyzed included the C-terminal TBD (residues 255−359), a

Table 1: Thermodynamic Parameters of the Interaction Between Cyclin T1 and Different Hexim1 Constructs As Determined by Isothermal Titration Calorimetry

protein variant[a]	T (°C)	$\Delta G°$ (kcal/mol)	$\Delta H°$ (kcal/mol)	$\Delta S°$ (cal mol^{-1} K^{-1})	K_D (μM)	molar ratio
Hexim1 (full-length)	15	−7.43	−13.07 ± 0.31	−19.6	2.3 ± 0.14	0.57 ± 0.01
TBD (wild-type)	15	−7.29	−12.79 ± 0.69	−19.1	2.9 ± 0.15	0.43 ± 0.02
TBD-Δstammer[b]	25	−6.66	−5.62 ± 0.44	3.5	13.5 ± 2.8	0.64 ± 0.04
TBD-VV	15	−7.41	−3.58 ± 0.33	13.3	2.4 ± 0.64	0.52 ± 0.03
TBD-short	15	−7.47	−6.31 ± 0.07	4.0	2.2 ± 0.14	1.00 ± 0.01
TBD-VVshort[b]	25	−6.62	−4.07 ± 0.32	8.5	14.0 ± 2.6	0.84 ± 0.04

[a]Cyclin T1 comprised the cyclin box domain encompassing residues 1−272. [b]The K_D values for TBD-Δstammer and TBD-VVshort remain the same when extrapolated to a temperature of 15 °C.

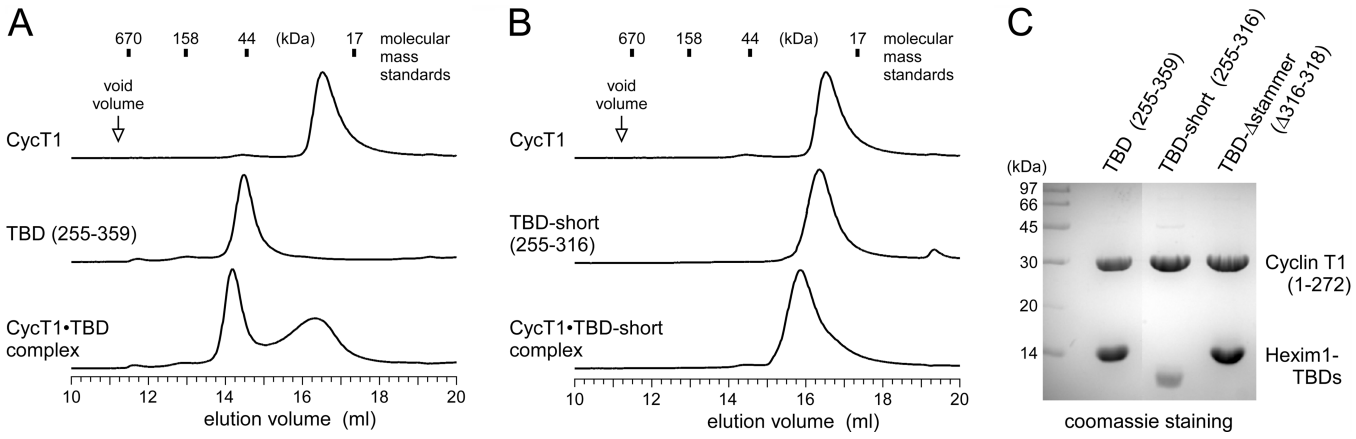

FIGURE 3: Size exclusion chromatography of formation of the complex of Hexim1 and CycT1. (A) Analytical gel filtration of the CycT1-TBD interaction. While CycT1(1−272) eluted at its expected size (top panel), the coiled coil TBD(255−359) migrated at early retention times due to its rigid and elliptically shaped structure (middle panels). When complexes were formed at equal molar ratios (bottom panel), a slight shift toward a higher-molecular mass complex was observed. In addition, excess CycT1 remained in the elution volume, suggesting a 1:2 binding stoichiometry rather than a 2:2 stoichiometry. (B) Same as panel A but with the Hexim1-TBD-short species. Again the elution profile of the complex does not suggest the formation of a 2:2 binding assembly (bottom panel). (C) SDS−PAGE analysis of formation of the complex of CycT1 and Hexim1-TBD, TBD-short, and TBD-Δstammer, which resulted from gel filtration experiments. Proteins were stained with Coomassie blue and analyzed using 20% acrylamide gels.

further reduction to only the first coiled coil segment of the TBD, named TBD-short (residues 255−316), and a deletion mutant TBD-Δstammer that omits the central GGD insert (residues 316−318) of three residues. Furthermore, two polar residues at heptad **a** positions in the first coiled coil segment (K284 and Y291) were mutated to β-branched valines that are favored for tight packing in a parallel coiled coil dimer structure (*26*). These two residues, K284 and Y291, are highly conserved in Hexim1 and Hexim2 orthologues from different species, suggesting a functional role in protein interactions. The double mutations were introduced both into the TBD, termed TBD-VV, and into the short variant of the TBD encompassing only the first coiled coil segment, termed TBD-VVshort. Human CycT1 comprised the N-terminal cyclin box domain encompassing residues 1−272 (Figure 1B). All proteins were expressed in *E. coli* and purified to homogeneity by affinity chromatography and size exclusion chromatography. An overview of the domain architecture of Hexim1 and the constructs analyzed is shown in Figure 1C.

Binding Affinity and Stoichiometry of the Hexim1−CycT1 Interaction. NMR chemical shift perturbation experiments and mutagenesis data both suggested a large interaction surface on the Hexim1-TBD structure for binding to CycT1 that covers the first coiled coil segment and part of the N-terminally adjacent helix (*22*). Previous studies showed that the cyclin box repeat region of CycT1 is sufficient for binding to Hexim1 and that residues outside this domain (290−726) do not contribute to the interaction with Hexim1 (*7*). We performed isothermal titration calorimetry measurements to study the binding affinity and stoichiometry of formation of the complex and to analyze if the first coiled coil segment is sufficient for the interaction. First, we titrated TBD or TBD-short into a solution of CycT1 placed in the sample cell and observed the heat current upon the interaction (Figure 2A). Both fragments showed a similar change in free energy ($\Delta G°$); the contribution of the entropy $T\Delta S$, however, differed significantly from 1.2 kcal/mol for TBD-short to −5.5 kcal/mol for the full-length TBD (Table 1). This change is compensated by different enthalpy values ($\Delta H°$) of −6.3 kcal/mol for TBD-short and −12.8 kcal/mol for TBD, yielding indeed similar free energy values ($\Delta G°$) of −7.5 and −7.3 kcal/mol, respectively. To our surprise, the stoichiometry differed markedly for the two complexes, resulting in molar ratios (N) of 0.43 for TBD−CycT1 binding and 1.00 for TBD-short−CycT1 binding (Table 1). This indicates that one Hexim1-TBD molecule contains approximately 0.5 binding site for CycT1, meaning that the dimeric coiled coil structure of the TBD binds one CycT1 molecule, while for TBD-short, the interaction with CycT1 is equimolar. The dissociation constants, however, appeared to be similar, with a K_D of 2.9 μM for the TBD and a K_D of 2.2 μM for TBD-short, suggesting that all binding determinants are within the range of residues 255−316.

As a reference, we used full-length Hexim1 (residues 1−359) for ITC measurements with CycT1 (Figure 2B). Enthalpy ($\Delta H^\circ = -13.1$ kcal/mol) and entropy ($T\Delta S^\circ = -5.6$ kcal/mol) values again yielded a similar free energy ($\Delta G^\circ = -7.4$ kcal/mol) for the binding and resulted in a dissociation constant of 2.3 μM as similarly observed for TBD and TBD-short. The molar ratio indicated again, as for TBD, a 1:2 binding stoichiometry for formation of the complex of CycT1 and native Hexim1, suggesting that twice as many Hexim1 molecules are required for formation of the full complex with CycT1. When the deletion mutant TBD-Δstammer was titrated to CycT1, we observed the same stoichiometry for formation of the complex as with the TBD; however, the dissociation constant was approximately 5-fold increased, indicating the importance of a bipartite coiled coil structure for the interaction (Table 1). In contrast, the double mutant TBD-VV (K284V/Y291V) showed no change in CycT1 binding affinity and stoichiometry compared to those of the wild-type TBD, while in combination with the short TBD-VVshort construct again an equimolar ratio of reduced affinity was measured. A summary of the ITC measurements performed and the purity of the proteins used for ITC and gel filtration experiments is shown in Figure 1 of the Supporting Information.

Size Exclusion Chromatography of Complex Formation. The observation of different binding stoichiometries for the various Hexim1 constructs leaves three possible explanations. Either TBD-short does not form a coiled coil structure but still binds CycT1. The dimeric coiled coil dissociates (fully or partially) upon binding, such that individual TBD helices bind CycT1. The complex of CycT1 and TBD-short is formed in a 2:2 assembly instead of a 1:1 complex. To further address this question, we performed size exclusion chromatography, cross-linking reactions, and analytical ultracentrifugation.

First, analytical gel filtration experiments were used to characterize complex formation. CycT1 and the Hexim1-TBD protein were applied to a Biosep S2000 column equilibrated in 50 mM Hepes buffer (Figure 3A). CycT1(1−272) with a molecular mass of 31.5 kDa eluted at 16.52 mL, while the dimeric TBD(255−359) with a molecular mass of 25 kDa appeared as an even larger molecule at 14.48 mL, which would correspond to an apparent mass of 46 kDa as calculated from the calibration standard. This observation is in line with previous results and a consequence of the elliptically shaped coiled coil structure of the TBD (*21*, *22*). Next, we applied the preformed complex of CycT1(1−272) and TBD(255−359) in equal monomer concentrations to the column. Now, the elution peak of the complex shifted toward earlier retention times (14.18 mL), indicating the increased size of the interacting proteins, while a significantly broadened elution peak for CycT1 remained. This co-elution profile suggested excess CycT1 and confirmed the proposed 1:2 complex ratio of CycT1 to TBD(255−359).

A similar set of experiments was performed with TBD-short molecules (Figure 3B). Even here, TBD-short eluted slightly earlier than CycT1 at 16.35 mL, corresponding to an apparent mass of 23 kDa. Stable, elliptical coiled coil structures are indeed known to elute early in gel filtration experiments, exhibiting a calculated mass that well exceeds the molecular mass when referenced to a calibration standard of globular proteins (*34*, *35*). Heteronuclear NMR experiments using ^{1}H- and ^{15}N-labeled TBD and TBD-short confirmed the helical structures by largely similar chemical shifts of the backbone atoms (data not shown). Now, the complex of CycT1 and TBD-short eluted slightly earlier at 15.85 mL, corresponding to an apparent molecular mass of 32 kDa. This complex size clearly indicated that a 2:2 heterodimer is not formed between CycT1 and TBD-short but a 1:1 assembly. An analysis of the protein composition of the peak eluates from the size exclusion chromatograms by SDS−PAGE confirmed the formation of CycT1−Hexim1 complexes (Figure 3C). From these experiments, we conclude that dimeric Hexim1 binds one CycT1 molecule while the short coiled coil TBD fragment dissociates upon binding to form an equimolar complex.

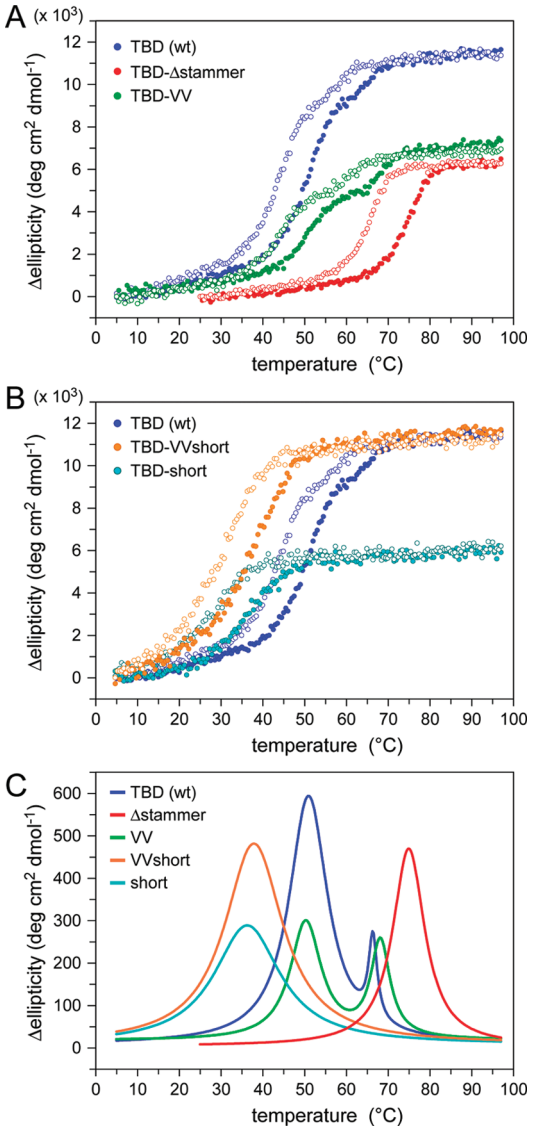

FIGURE 4: Thermal denaturation experiments of Hexim1-TBD proteins monitored by circular dichroism spectroscopy. (A) Thermal denaturation and renaturation profiles of TBD (wild-type), TBD-VV, and TBD-Δstammer. CD measurements were performed by recording the molar ellipticity at 222 nm from 5 to 95 °C at a heating and cooling rate of 5.0 K/min. Protein concentrations were set to 5 μM. Filled circles indicate the heating phase and empty circles the cooling phase. Note that TBD (wild-type) and TBD-VV exhibit two separate melting transitions, in agreement with two distinct coiled coil segments, while TBD-Δstammer appeared significantly more stable with only one melting phase. (B) De- and renaturation profiles of TBD (wild-type), TBD-short, and TBD-VVshort. CD spectra were measured as described for panel A. The stability of the single coiled coil segment in the TBD-short constructs was significantly reduced compared to that of the wild type. (C) Display of the first derivative of the denaturation curves and the corresponding line fit as a function of temperature. The curves were fitted to a single or double Lorentzian line for the determination of the melting temperatures.

Stability of the Hexim1 Coiled Coil Segments. The thermal stability of the coiled coil structure of Hexim1 was next assayed by circular dichroism spectroscopy. The mean residue ellipticity of the five TBD variants measured in the far-UV spectrum from 250 to 190 nm at protein concentrations of 5 μM indicated the integrity of the helical structures (data not shown). Next, the mean residual ellipticity was measured at 222 nm in a heating−cooling cycle from 5 to 97 °C for all TBD samples (Figure 4). Surprisingly, none of the proteins precipitated during the heating cycle despite the high end point temperature of 97 °C, potentially due to the highly polar protein sequence of 40% charged residues in the wild-type TBD. The coiled coil chains renatured upon cooling with a lag phase of typically 7−8 °C against denaturing. TBD and TBD-VV exhibited two separable transitions both in the denaturing cycle and in the renaturing cycle, suggesting two distinct melting processes of the two coiled coil segments (Figure 4A). In contrast, TBD-Δstammer exhibited only one melting phase that is shifted against the first denaturation process of the wild-type TBD by more than 20 °C toward a higher temperature (Table 2). This observation suggests a homogeneous structure of the TBD-Δstammer construct of increased stability, in line with the assumption of a continuous monopartite coiled coil domain.

Table 2: Melting Temperatures of Hexim1-TBD Constructs As Determined by CD Spectroscopy

protein variant	first T_m (°C)	second T_m (°C)
TBD (wild-type)	51	66
TBD-Δstammer	–	75
TBD-VV	50	68
TBD-short	36	–
TBD-VVshort	38	–

Similarly, the truncated Hexim1 constructs TBD-short and TBD-VVshort exhibited only one denaturing process at lower melting temperatures (Figure 4B). Interestingly, in both constructs, the VV mutation led to no increase or only a small increase in the stability of the coiled coil structure. The individual melting temperatures were determined by a single or double Lorentzian line fit to the first derivative of the ellipticity as a function of temperature (Figure 4C). The fitted melting temperatures are listed in Table 2. The large increase in stability of the TBD-Δstammer variant and the reduction to single melting phases for the TBD-short variant thus correlate well with the structure of a bipartite coiled coil segment for the Hexim1-TBD protein.

Chemical Cross-Linking of the Cyclin T1−Hexim1 Complex. To determine the stoichiometry of a macromolecular complex assembly, most methods rely on the accuracy of the protein concentration determination. Typically, the protein concentration is obtained by either a Bradford assay or photometric absorption measurement at 280 nm, which sometimes results in significantly different concentration values. This is an inherent problem in the analysis of stoichiometry data obtained, for example, via isothermal titration calorimetry or fluorescence-based techniques. Similarly, the electrophoretic migration in gels as well as the elution time in size exclusion chromatography and the sedimentation constant in analytical ultracentrifugation depend not only on the molecular mass but also on the shape of the proteins analyzed. To bypass these issues, we used chemical cross-linking experiments for the analysis of the CycT1−Hexim1 complex (Figure 5). After destroying the tertiary and secondary structure by heat and SDS, this method allows the observation of the protein complex stoichiometry in a denatured state of the components and is thus independent of the shape of protein complexes. Bis(sulfosuccinimidyl)suberate (BS^3), a water-soluble *N*-hydroxysuccinimide ester, was used as cross-linking reagent

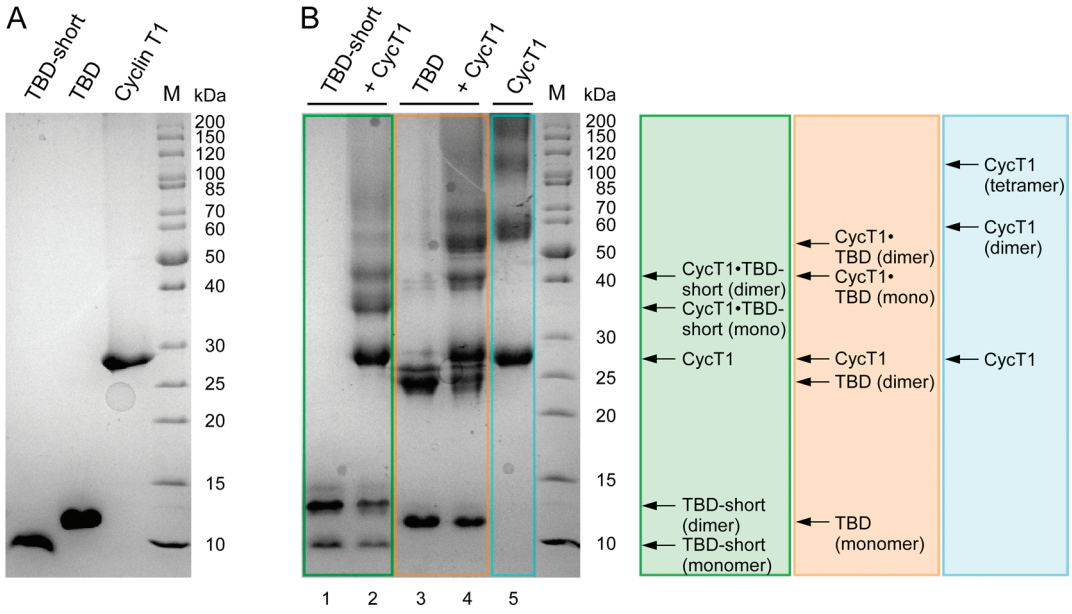

FIGURE 5: Comparison of the cross-linking reactions of CycT1 with Hexim1-TBD or TBD-short by SDS−PAGE. (A) Input controls of Hexim1-TBD, TBD-short, and CycT1 without cross-linking reagents. (B) Cross-linking of CycT1 and Hexim1 with BS^3. The left box shows the incubation of TBD-short alone or in complex with CycT1. The highest prominent migration band appeared at 45 kDa, corresponding to one CycT1 molecule bound to a TBD-short dimer. The middle box shows cross-linking of TBD alone or in complex with CycT1. The most prominent migration band appeared shortly above 50 kDa and is suited best to one CycT1 protein in a complex with a TBD dimer. Importantly, no migration band was detected that would correspond to a 2:2 CycT1−Hexim1 complex. In the right box, cross-linking of CycT1 alone showed a predominantly monomeric conformation with decreasing contributions of dimer and tetramer assemblies. The assignments of the Coomassie-stained bands are given at the right.

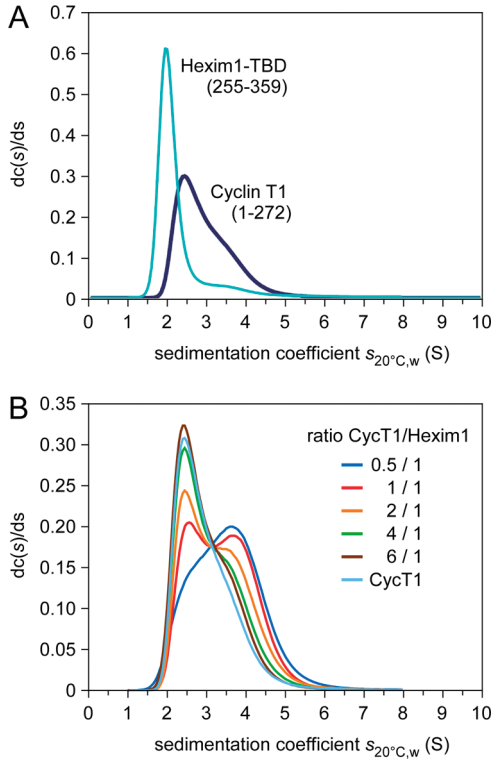

FIGURE 6: Analytical ultracentrifugation of Hexim1, CycT1, and complexes thereof. (A) Differential sedimentation coefficient distributions for Hexim1-TBD and CycT1. Sedimentation profiles were calculated from sedimentation traces of 9 μM Hexim1-TBD in 50 mM Hepes buffer (pH 7.5), 100 mM KCl, and 1 mM DTE or 9 μM CycT1(1−272) using SEDFIT (*32*). The TBD existed in a single fraction at 1.97 S, corresponding to an apparent molecular mass of 26.7 kg/mol indicating a dimeric state. CycT1 prevails in a monomeric conformation at 2.6 S, with some extended to an aggregated state at 3.7 S. (B) Differential sedimentation coefficient distributions of a titration series of CycT1 to Hexim1-TBD at molar ratios of 0.5, 1, 2, 4, and 6. The prevailing fraction at 4.2 S in the initial profile indicated formation of the heteromolecular complex. Addition of CycT1 suggested the appearance of excess CycT1 that is not incorporated into the complex with Hexim1 already at an equal molar ratio (red line).

for coupling CycT1(1−272) in a complex with either Hexim1-TBD(255−359) or TBD-short(255−316). The BS^3 cross-linker reacts with primary amino groups ($-NH_3$), such as the side chains of lysine residues or the protein's N-termini, to form stable amide bonds.

For comparison, the input controls of non-cross-linked Hexim1 TBD-short(255−316), TBD(255−359), and CycT1-(1−272) are shown in the Coomassie-stained SDS−PAGE gel (Figure 5A). All proteins appeared at the expected size corresponding to their molecular masses of 7.5, 12.5, and 30.5 kDa, respectively. CycT1 and Hexim1 protein samples were then mixed in an equimolecular concentration ratio. After incubation of the cross-linking reaction mixture for 30 min at room temperature, protein samples were subjected to SDS−PAGE analyses (Figure 5B). Now, TBD-short prevailed in a dimeric state (15 kDa) while no higher-molecular mass oligomers were observed (lane 1). Upon addition of CycT1, monomers and dimers of TBD-short were diminished, while a complex of CycT1 with one Hexim moiety and with a Hexim dimer appeared at 38 and 45.5 kDa, respectively (lane 2). Similarly, the TBD appeared as a monomer and dimer after the cross-linking experiment (lane 3). In complex with CycT1, a prominent band at 56 kDa and a second band at 43 kDa of reduced intensity were observed, indicating the 1:2 and 1:1 formation of the CycT1−Hexim1-TBD heterocomplex (lane 4). Of note, the band indicating the 1:1 molar ratio for the interaction of CycT1 with TBD-short prevailed, while for the interaction with TBD, the 1:2 ratio was strongest (compare lanes 2 and 4). This observation is in line with results from ITC and size exclusion chromatography.

When CycT1 alone was subjected to the cross-linking procedure, it appeared to be mainly monomeric, but bands at 61 and 122 kDa corresponding to dimers and tetramers, respectively, could also be identified (lane 5). Since CycT1 appeared neither in the crystal structure (*29*) nor in complex with Cdk9 (*27*) or Tat-TAR (*36*) as a dimer, these oligomers may result from unspecific aggregations of the cyclin box domain. Importantly, in the heteromolecular complex assays, no high-molecular mass bands at 76 kDa for TBD-short (lane 2) or at 86 kDa for TBD (lane 4) could be observed that would correspond to the assembly of a Hexim dimer with two CycT1 molecules. While such 2:2 stoichiometries could not be observed, it rather appeared that the unspecific aggregation of CycT1 was weakened by the presence of the interaction partner Hexim1.

Analytical Ultracentrifugation Indicates a Low-Molecular Mass Complex. Finally, sedimentation velocity analysis in the analytical ultracentrifuge was used to characterize the CycT1−Hexim1 complex. A 122 μM concentrated Hexim1−TBD protein sample was sedimented at 43000 rpm and 20 °C. The differential sedimentation coefficient distributions showed for Hexim1-TBD a sedimentation behavior corresponding to a uniform species at 1.97 S (Figure 6A). With a molecular mass of 26.7 kg/mol, a friction coefficient (Perrin) of 1.65 is obtained, showing that this species can be described well as a nonglobular dimer. In contrast, CycT1(1−272) appeared less uniform with a major fraction at 2.45 S and some faster-sedimenting aggregates.

Next, CycT1 was titrated in increasing amounts at molar ratios of 0.5, 1, 2, 4, and 6 to Hexim1-TBD. Formation of a complex of CycT1 and Hexim-TBD led to the appearance of a reaction boundary sedimenting faster than any of the two components alone (Figure 6B). The fastest reaction boundary sedimenting at 3.7 S is already formed under the starting conditions with a 1:2 molar ratio of CycT1 to Hexim1-TBD (Figure 6B, blue line). Further addition of CycT1 did not lead to an increase in the sedimentation rate of this reaction boundary. Instead, an increase in the level of free CycT1 at 2.45 S was observed (all other lines). Thus, no Hexim1-TBD complexes containing more than a single CycT1 molecule could be observed via analytical ultracentrifugation. In addition, no sedimentation boundary corresponding to free Hexim1-TBD at 1.97 S was observed under the starting conditions with a 1:2 molar ratio indicating strong binding. The titration series performed by analytical ultracentrifugation therefore indicates that formation of the complex of CycT1 and Hexim1 occurs with a 1:2 molar ratio.

DISCUSSION

The analysis of the stability of the two coiled coil segments in Hexim1 and their individual contribution to the interaction with the cyclin box domain of CycT1 suggests that the first coiled coil region is required for binding to the P-TEFb subunit while the second coiled coil segment keeps Hexim1 dimeric. Notably, we found that the symmetrical coiled coil dimer of Hexim1 coordinates one CycT1 molecule (not two). This observation extends

previous reports based on experiments with HeLa cell extracts loaded on glycerol gradients and size exclusion columns that suggested a 2:2 heterodimer of Hexim1 and CycT1/Cdk9 (*37*, *38*). Moreover, the 67 kDa Larp7 protein was identified in the mean time as an additional cofactor of the scaffolding 7SK RNA in the large inhibited complex. Larp7 directly interacts with 7SK, Hexim1, and Cdk9 and is thought to stabilize the RNA structure by multiple interactions (*9*−*11*, *39*). Since only one 7SK RNA was supposed to reside in the inhibited P-TEFb complex (*37*), we propose that the large inhibited P-TEFb complex consists of a 1:1:2:1:1 Cdk9−CycT1−Hexim1−7SK−Larp7 subunit assembly. In addition, a stoichiometric assembly of the 5′ RNA methylating enzyme BCDIN3 (or MePCE) with 7SK was recently described that could further contribute to the molecular mass of the native complex (*40*−*42*).

Circular dichroism measurements suggested that the first coiled coil segment of Hexim1-TBD is structurally independent and folds in the absence of the second. Consistent with the presence of only one instead of two coiled coil regions, TBD-short exhibited only a single unfolding transition. The T_m value of this transition is lower than that of the first melting point of the full TBD, indicating a lowered stability of the first coiled coil segment in the absence of the second (Table 2). TBD-short binds CycT1 with approximately the same affinity (K_D = 2.2 μM) as TBD or the full-length Hexim1 protein; however, the stoichiometry changes from a 2:1 Hexim1−CycT1 complex of the full-length form or the TBD to an equimolar complex assembly for the TBD-short variant. This observation suggests that the C-terminal second coiled coil in the TBD acts as a clamp that keeps Hexim1 dimeric upon interacting with CycT1 and allows only the formation of an asymmetric 2:1 complex. Furthermore, the formation of a 1:1 but not a 2:2 complex for TBD-short indicates that the first segment dissociates upon the interaction with CycT1, which may indicate that the first coiled coil is more flexible in conformation and less stable than the second. Indeed, many native coiled coil proteins contain a small fraction of polar residues at core forming positions that are important for their structural and functional specificity, albeit at the price of reduced stability (*23*, *24*).

The K284V and Y291V mutations were expected to stabilize the structural fold of the first coiled coil segment. On the basis of the data recorded from CD measurements and size exclusion chromatography experiments, both proteins maintain the homodimeric coiled coil structure of the wild-type protein, yet the increase in stability as monitored by thermal unfolding appeared to be only very moderate for TBD-VV and TBD-VVshort. This observation suggests that the long aliphatic side chains of both native residues K284 and Y291 contribute readily to the stability at position **a** of the coiled coil interface and that the polar headgroups do not disturb this assembly substantially. TBD-VV showed an affinity for CycT1 similar to that of the wild-type TBD; however, the entropic and enthalpic contributions were very different (Table 1). Therefore, the divergences in the first coiled coil segment from an evolutionarily conserved sequence composition seem to be important for the specific interaction of Hexim1 with CycT1.

The 2:1 stoichiometry of formation of the Hexim1−CycT1 complex observed by ITC, analytical gel filtration, cross-linking experiments, and analytical ultracentrifugation could result from the steric hindrance of the symmetry-related second binding site, e.g., by gathering the coiled coil structure into a recognition site on the cyclin box domain that renders the second site nonaccessible. Alternatively, the unequal stoichiometry could be a consequence of the initiation of a molecular asymmetry, such as the interaction of a third heterologous helix with the coiled coil dimer. Such a binding mode has been reported recently for the interaction of cytokinesis factor ALIX with protein CEP55 from the midbody targeting machinery (*43*). Similarly, dimeric guanosine exchange factor Sec2p from yeast that forms a parallel coiled coil structure binds the Rab GTPase Sec4p in a 2:1 ratio (*44*, *45*). Likewise, transitions in the helical coiled coil assembly could occur as shown, for example, for the signal transduction mechanism of the HAMP domain (*46*). It could be envisioned that a helix from CycT1 complements the first noncanonical coiled coil segment of Hexim1, e.g., by forming a mixed three-strand helical bundle. The C-terminal coiled coil segment instead, which is not involved in CycT1 binding, would keep the two Hexim1 strains together. This model is supported by the observation that a short TBD fragment whose second coiled coil segment was truncated loses its dimeric structure upon binding to CycT1, although it retains a similar binding affinity. Thermal denaturation experiments with various TBD variants showed that the region around α1 and α2 is less rigid than the succeeding coiled coil segment. Further structural studies will be required for the analysis of formation of the complex of Cdk9, CycT1, and Hexim1 to elucidate the mechanism of P-TEFb inhibition.

ACKNOWLEDGMENT

We thank Diana Ludwig for expert technical assistance. A.S., J.M.B., and M.G. acknowledge Roger Goody for continuous support.

SUPPORTING INFORMATION AVAILABLE

Additional ITC measurements as described in the text and SPS−PAGE analysis of the proteins applied. This material is available free of charge via the Internet at http://pubs.acs.org.

REFERENCES

1. Saunders, A., Core, L. J., and Lis, J. T. (2006) Breaking barriers to transcription elongation. *Nat. Rev. Mol. Cell Biol. 7*, 557–567.
2. Margaritis, T., and Holstege, F. C. (2008) Poised RNA polymerase II gives pause for thought. *Cell 133*, 581–584.
3. Peterlin, B. M., and Price, D. H. (2006) Controlling the elongation phase of transcription with P-TEFb. *Mol. Cell 23*, 297–305.
4. Zhou, Q., and Yik, J. H. (2006) The Yin and Yang of P-TEFb regulation: Implications for human immunodeficiency virus gene expression and global control of cell growth and differentiation. *Microbiol. Mol. Biol. Rev. 70*, 646–659.
5. Wada, T., Takagi, T., Yamaguchi, Y., Watanabe, D., and Handa, H. (1998) Evidence that P-TEFb alleviates the negative effect of DSIF on RNA polymerase II-dependent transcription *in vitro*. *EMBO J. 17*, 7395–7403.
6. Ping, Y. H., and Rana, T. M. (2001) DSIF and NELF interact with RNA polymerase II elongation complex and HIV-1 Tat stimulates P-TEFb-mediated phosphorylation of RNA polymerase II and DSIF during transcription elongation. *J. Biol. Chem. 276*, 12951–12958.
7. Michels, A., Nguyen, V., Fraldi, A., Labas, V., Edwards, M., Bonnet, F., Lania, L., and Bensaude, O. (2003) MAQ1 and 7SK RNA interact with CDK9/cyclin T complexes in a transcription-dependent manner. *Mol. Cell. Biol. 23*, 4859–4869.
8. Yik, J. H., Chen, R., Nishimura, R., Jennings, J. L., Link, A. J., and Zhou, Q. (2003) Inhibition of P-TEFb (CDK9/Cyclin T) kinase and RNA polymerase II transcription by the coordinated actions of HEXIM1 and 7SK snRNA. *Mol. Cell 12*, 971–982.
9. He, N., Jahchan, N. S., Hong, E., Li, Q., Bayfield, M. A., Maraia, R. J., Luo, K., and Zhou, Q. (2008) A La-related protein modulates 7SK snRNP integrity to suppress P-TEFb-dependent transcriptional elongation and tumorigenesis. *Mol. Cell 29*, 588–599.

10. Krueger, B. J., Jeronimo, C., Roy, B. B., Bouchard, A., Barrandon, C., Byers, S. A., Searcey, C. E., Cooper, J. J., Bensaude, O., Cohen, E. A., Coulombe, B., and Price, D. H. (2008) LARP7 is a stable component of the 7SK snRNP while P-TEFb, HEXIM1 and hnRNP A1 are reversibly associated. *Nucleic Acids Res. 36*, 2219–2229.
11. Markert, A., Grimm, M., Martinez, J., Wiesner, J., Meyerhans, A., Meyuhas, O., Sickmann, A., and Fischer, U. (2008) The La-related protein LARP7 is a component of the 7SK ribonucleoprotein and affects transcription of cellular and viral polymerase II genes. *EMBO Rep. 9*, 569–575.
12. Egloff, S., Van Herreweghe, E., and Kiss, T. (2006) Regulation of polymerase II transcription by 7SK snRNA: Two distinct RNA elements direct P-TEFb and HEXIM1 binding. *Mol. Cell. Biol. 26*, 630–642.
13. Li, Q., Cooper, J. J., Altwerger, G. H., Feldkamp, M. D., Shea, M. A., and Price, D. H. (2007) HEXIM1 is a promiscuous double-stranded RNA-binding protein and interacts with RNAs in addition to 7SK in cultured cells. *Nucleic Acids Res. 35*, 2503–2512.
14. Bélanger, F., Baigude, H., and Rana, T. M. (2009) U30 of 7SK RNA forms a specific photo-cross-link with Hexim1 in the context of both a minimal RNA-binding site and a fully reconstituted 7SK/Hexim1/P-TEFb ribonucleoprotein complex. *J. Mol. Biol. 386*, 1094–1107.
15. Czudnochowski, N., Vollmuth, F., Baumann, S., Vogel-Bachmayr, K., and Geyer, M. (2010) Specificity of Hexim1 and Hexim2 complex formation with Cyclin T1/T2, Importin α and 7SK snRNA. *J. Mol. Biol. 395*, 28–41.
16. Bisgrove, D., Mahmoudi, T., Henklein, P., and Verdin, E. (2007) Conserved P-TEFb-interacting domain of BRD4 inhibits HIV transcription. *Proc. Natl. Acad. Sci. U.S.A. 104*, 13690–13695.
17. Jang, M., Mochizuki, K., Zhou, M., Jeong, H., Brady, J., and Ozato, K. (2005) The bromodomain protein Brd4 is a positive regulatory component of P-TEFb and stimulates RNA polymerase II-dependent transcription. *Mol. Cell 19*, 523–534.
18. Yang, Z., Yik, J., Chen, R., He, N., Jang, M., Ozato, K., and Zhou, Q. (2005) Recruitment of P-TEFb for stimulation of transcriptional elongation by the bromodomain protein Brd4. *Mol. Cell 19*, 535–545.
19. Vollmuth, F., Blankenfeldt, W., and Geyer, M. (2009) Structures of the dual bromodomains of the P-TEFb-activating protein Brd4 at atomic resolution. *J. Biol. Chem. 284*, 36547–36556.
20. Michels, A., Fraldi, A., Li, Q., Adamson, T., Bonnet, F., Nguyen, V., Sedore, S., Price, J., Price, D. H., Lania, L., and Bensaude, O. (2004) Binding of the 7SK snRNA turns the HEXIM1 protein into a P-TEFb (CDK9/cyclin T) inhibitor. *EMBO J. 23*, 2608–2619.
21. Schulte, A., Czudnochowski, N., Barboric, M., Schönichen, A., Blazek, D., Peterlin, B. M., and Geyer, M. (2005) Identification of a cyclin T-binding domain in Hexim1 and biochemical analysis of its binding competition with HIV-1 Tat. *J. Biol. Chem. 280*, 24968–24977.
22. Dames, S., Schönichen, A., Schulte, A., Barboric, M., Peterlin, B. M., Grzesiek, S., and Geyer, M. (2007) Structure of the Cyclin T binding domain of Hexim1 and molecular basis for its recognition of P-TEFb. *Proc. Natl. Acad. Sci. U.S.A. 104*, 14312–14317.
23. Lupas, A. N., and Gruber, M. (2005) The structure of α-helical coiled coils. *Adv. Protein Chem. 70*, 37–78.
24. Mason, J. M., and Arndt, K. M. (2004) Coiled coil domains: Stability, specificity, and biological implications. *ChemBioChem 5*, 170–176.
25. Brown, J. H., Cohen, C., and Parry, D. A. (1996) Heptad breaks in α-helical coiled coils: Stutters and stammers. *Proteins 26*, 134–145.
26. Woolfson, D. N. (2005) The design of coiled-coil structures and assemblies. *Adv. Protein Chem. 70*, 79–112.
27. Baumli, S., Lolli, G., Lowe, E. D., Troiani, S., Rusconi, L., Bullock, A. N., Debreczeni, J. E., Knapp, S., and Johnson, L. N. (2008) The structure of P-TEFb (CDK9/cyclin T1), its complex with flavopiridol and regulation by phosphorylation. *EMBO J. 27*, 1907–1918.
28. Breuer, S., Gerlach, H., Kolaric, B., Urbanke, C., Opitz, N., and Geyer, M. (2006) Biochemical indication for myristoylation-dependent conformational changes in HIV-1 Nef. *Biochemistry 45*, 2339–2349.
29. Anand, K., Schulte, A., Fujinaga, K., Scheffzek, K., and Geyer, M. (2007) Cyclin box structure of the P-TEFb subunit cyclin T1 derived from a fusion complex with EIAV Tat. *J. Mol. Biol. 370*, 826–836.
30. Schönichen, A., Alexander, M., Gasteier, J. E., Cuesta, F. E., Fackler, O. T., and Geyer, M. (2006) Biochemical characterization of the diaphanous autoregulatory interaction in the formin homology protein FHOD1. *J. Biol. Chem. 281*, 5084–5093.
31. Pylypenko, O., Schönichen, A., Ludwig, D., Ungermann, C., Goody, R. S., Rak, A., and Geyer, M. (2008) Farnesylation of the SNARE protein Ykt6 increases its stability and helical folding. *J. Mol. Biol. 377*, 1334–1345.
32. Lebowitz, J., Lewis, M. S., and Schuck, P. (2002) Modern analytical ultracentrifugation in protein science: A tutorial review. *Protein Sci. 11*, 2067–2079.
33. Laue, T. M., Shah, D. B., Ridgeway, T. M., and Pelletier, S. L. (1992) Computer-aided interpretation of analytical sedimentation data for proteins. In Analytical Ultracentrifugation in Biochemistry and Protein Science (Harding, S. E., Rowe, A. J., and Horton, J. C., Eds.) pp 90−125, The Royal Society of Chemistry, Cambridge, U.K.
34. Erickson, H. P. (2009) Size and Shape of Protein Molecules at the Nanometer Level Determined by Sedimentation, Gel Filtration, and Electron Microscopy. In Biological Procedures Online (Li, S., Ed.) Vol. *11*, pp 32−51, Springer, New York.
35. Bergbrede, T., Chuky, N., Schoebel, S., Blankenfeldt, W., Geyer, M., Fuchs, E., Goody, R. S., Barr, F., and Alexandrov, K. (2009) Biophysical analysis of the interaction of Rab6a GTPase with its effector domains. *J. Biol. Chem. 284*, 2628–2635.
36. Anand, K., Schulte, A., Vogel-Bachmayr, K., Scheffzek, K., and Geyer, M. (2008) Structural insights into the cyclin T1-Tat-TAR RNA transcription activation complex from EIAV. *Nat. Struct. Mol. Biol. 15*, 1287–1292.
37. Li, Q., Price, J., Byers, S., Cheng, D., Peng, J., and Price, D. H. (2005) Analysis of the large inactive P-TEFb complex indicates that it contains one 7SK molecule, a dimer of HEXIM1 or HEXIM2, and two P-TEFb molecules containing Cdk9 phosphorylated at threonine 186. *J. Biol. Chem. 280*, 28819–28826.
38. Dulac, C., Michels, A. A., Fraldi, A., Bonnet, F., Nguyen, V. T., Napolitano, G., Lania, L., and Bensaude, O. (2005) Transcription-dependent association of multiple positive transcription elongation factor units to a HEXIM multimer. *J. Biol. Chem. 280*, 30619–30629.
39. Michels, A. A., and Bensaude, O. (2008) RNA-driven cyclin-dependent kinase regulation: When CDK9/cyclin T subunits of P-TEFb meet their ribonucleoprotein partners. *Biotechnol. J. 3*, 1022–1032.
40. Jeronimo, C., Forget, D., Bouchard, A., Li, Q., Chua, G., Poitras, C., Thérien, C., Bergeron, D., Bourassa, S., Greenblatt, J., Chabot, B., Poirier, G. G., Hughes, T. R., Blanchette, M., Price, D. H., and Coulombe, B. (2007) Systematic analysis of the protein interaction network for the human transcription machinery reveals the identity of the 7SK capping enzyme. *Mol. Cell 27*, 262–274.
41. Barboric, M., Lenasi, T., Chen, H., Johansen, E. B., Guo, S., and Peterlin, B. M. (2009) 7SK snRNP/P-TEFb couples transcription elongation with alternative splicing and is essential for vertebrate development. *Proc. Natl. Acad. Sci. U.S.A. 106*, 7798–7803.
42. Xue, Y., Yang, Z., Chen, R., and Zhou, Q. (2010) A capping-independent function of MePCE in stabilizing 7SK snRNA and facilitating the assembly of 7SK snRNP. *Nucleic Acids Res. 38*, 360–369.
43. Lee, H. H., Elia, N., Ghirlando, R., Lippincott-Schwartz, J., and Hurley, J. H. (2008) Midbody targeting of the ESCRT machinery by a noncanonical coiled coil in CEP55. *Science 322*, 576–580.
44. Sato, Y., Fukai, S., Ishitani, R., and Nureki, O. (2007) Crystal structure of the Sec4p.Sec2p complex in the nucleotide exchanging intermediate state. *Proc. Natl. Acad. Sci. U.S.A. 104*, 8305–8310.
45. Dong, G., Medkova, M., Novick, P., and Reinisch, K. M. (2007) A catalytic coiled coil: Structural insights into the activation of the Rab GTPase Sec4p by Sec2p. *Mol. Cell 25*, 455–462.
46. Hulko, M., Berndt, F., Gruber, M., Linder, J. U., Truffault, V., Schultz, A., Martin, J., Schultz, J. E., Lupas, A. N., and Coles, M. (2006) The HAMP domain structure implies helix rotation in transmembrane signaling. *Cell 126*, 929–940.